Nanozymes Hot Paper

Ligand-Dependent Activity Engineering of Glutathione Peroxidase-Mimicking MIL-47(V) Metal–Organic Framework Nanozyme for Therapy

Jiangjiexing Wu+, Yijun Yu+, Yuan Cheng+, Chaoqun Cheng, Yihong Zhang, Bo Jiang, Xiaozhi Zhao, Leiying Miao, and Hui Wei*

Abstract: Glutathione peroxidase (GPx) plays an important role in maintaining the reactive oxygen metabolic balance, yet limited GPx-mimicking nanozymes are currently available for in vivo therapy. Herein, a ligand engineering strategy is developed to modulate the GPx-mimicking activity of a metal–organic framework (MOF) nanozyme. With different substituted ligands, the GPx-mimicking activities of MIL-47(V)-X (MIL stands for Materials of Institute Lavoisier; X = F, Br, NH₂, CH₃, OH, and H) MOFs are rationally regulated. With the best one as an example, both in vitro and in vivo experiments reveal the excellent antioxidation ability of MIL-47(V)-NH₂, which alleviates the inflammatory response effectively for both ear injury and colitis, and is more active than MIL-47(V). This study proves that high-performance GPx-mimicking nanozymes can be rationally designed by a ligand engineering strategy, and that structure–activity relationships can direct the in vivo therapy. This study enriches nanozyme research and expands the range of biomimetic MOFs.

Introduction

Reactive oxygen species (ROS), such as superoxide and hydrogen peroxide (H_2O_2), are well known to contribute to various intracellular functions. Therefore, any cellular redox imbalance with elevated levels of ROS would cause oxidative damage to living cells and lead to various disorders in the long term.[1] Among cellular ROS, H_2O_2 plays a crucial role. H_2O_2 is not only longer lived as compared to superoxide, it can also easily diffuse or transfer across lipid membranes and is a precursor to the highly damaging hydroxyl radical.[1,2] Consequently, modulating intracellular ROS levels, especially the H_2O_2 level, below the toxic threshold is important for protecting cells from oxidative damage. In biological systems,

several antioxidation enzymes, including glutathione peroxidase (GPx) and catalase, are capable of converting H_2O_2 to benign H_2O to limit harmful effects. Of these, GPx has received a lot of attention, leading to its investigation in many disease therapies, such as cancer, inflammation, and cardiovascular disease.[3]

Although GPx plays a critical role in maintaining intracellular redox balance, it suffers from some limitations common to most natural enzymes, namely low stability and poor availability, which have limited its practical biomedical applications. To overcome these limitations, considerable effort has been devoted to developing GPx mimics.[4] Of these mimics, nanozymes, nanomaterials with enzyme-mimicking activities, have attracted much attention in recent years due to their exceptional advantages, such as low cost, large surface area, and robustness under extreme conditions.[5] In fact, several types of nanozymes, including peroxidase-, oxidase-, and catalase-mimicking nanozymes, have been developed and applied in bioanalysis and diagnosis, as well as numerous disease therapies.[6] However, few applications of GPx-mimicking nanozymes in therapy have been reported despite the critical role GPx plays in maintaining the reactive oxygen metabolic balance and protecting against injury by removing the excess H_2O_2. The reason for this relative dearth of applications is that limited types of nanozymes (only vanadium, manganese, and selenium-containing nanozymes listed in Table S1 in the Supporting Information) were reported to exhibit GPx-mimicking activities.[7] And their moderate activities required their coupling with other antioxidants to maintain the reactive oxygen metabolic balance in vivo.[8] The discovery of highly efficient GPx-mimicking V_2O_5 nanozymes was a breakthrough,[7a,9] though the exploration of high-performance GPx-mimicking nanozymes is still in an early stage and application of high-performance GPx-mimicking

[*] Dr. J. Wu,[+] Dr. Y. Cheng,[+] C. Cheng, Y. Zhang, Prof. H. Wei
Department of Biomedical Engineering, College of Engineering and Applied Sciences, Nanjing National Laboratory of Microstructures, Jiangsu Key Laboratory of Artificial Functional Materials, Chemistry and Biomedicine Innovation Center (ChemBIC), Nanjing University
Nanjing, Jiangsu 210093 (China)
E-mail: weihui@nju.edu.cn

Y. Yu,[+] Prof. L. Miao
Department of Cariology and Endodontics, Nanjing Stomatological Hospital, Medical School of Nanjing University, Nanjing University
Nanjing, Jiangsu 210093 (China)

Dr. B. Jiang, Dr. X. Zhao
Department of Urology, Drum Tower Hospital, Medical School of Nanjing University, Institute of Urology, Nanjing University
Nanjing, Jiangsu 210008 (China)

Prof. H. Wei
State Key Laboratory of Analytical Chemistry for Life Science and State Key Laboratory of Coordination Chemistry, School of Chemistry and Chemical Engineering, Nanjing University
Nanjing, Jiangsu 210093 (China)

[+] These authors contributed equally to this work.

Supporting information and the ORCID identification number(s) for the author(s) of this article can be found under:
https://doi.org/10.1002/anie.202010714.

nanozymes alone for in vivo therapy has not yet been accomplished.

Metal–organic frameworks (MOF) are a class of porous materials hybridized by metal nodes and multidentate organic linkers. MOFs possess large surface areas and a highly modular structure making them widely useful in gas adsorption, chemical sensing, heterogeneous catalysis, and so on.[10] Recently, biomimetic MOFs have attracted great attention and have been actively explored in mimicking hydrolase, peroxidase, and so on.[11] However, no MOFs have been reported to specifically mimic GPx nor applied alone as an antioxidation defense against inflammation in vivo. Herein, inspired by protein engineering, we reason that the shared metal–ligand coordination of natural metalloenzymes and MOFs will enable us to rationally modulate the enzyme-mimicking activity of MOFs via a ligand engineering strategy. Specifically, we intentionally modulated the GPx-mimicking activities of MIL-47(V)-X (MIL stands for Materials of Institute Lavoisier) MOFs by varying the substitution of H in the 1,4-benzenedicarboxylicacid (BDC) ligand with F, Br, NH_2, CH_3, and OH. The corresponding isostructural MOFs are named as MIL-47(V)-H, MIL-47(V)-F, MIL-47(V)-Br, MIL-47(V)-NH_2, MIL-47(V)-CH_3, and MIL-47(V)-OH, respectively (Figure 1). The substitution tunes the electronic properties of the BDC ligand and thus fine-tunes the enzymatic activities. Among these isostructural MOFs of MIL-47(V)-X, MIL-47(V)-NH_2 exhibits the highest GPx-

mimicking activity. Furthermore, its excellent in vitro anti-oxidation ability in reducing ROS level and in vivo protection from ear-inflammation and colitis are also demonstrated.

Results and Discussion

MIL-47(V)-X (X = F, Br, NH_2, CH_3, OH, and H) is assembled from vanadium metal nodes and terephthalate linkers (substituted terephthalate linkers, Figure 1), forming 1D cavities in the final framework.[12] The synthesis of MIL-47(V)-X MOFs was carried out by a microwave method, as previously reported.[13] Various characterization techniques were performed for MIL-47(V)-X MOFs. As shown in Figure 2A, the powder X-ray diffraction (PXRD) patterns of MIL-47(V)-X MOFs were in accordance with literature results,[14] confirming the successful preparation of the MIL-47(V)-X MOFs. The thermogravimetric analysis (TGA; Supporting Information, Figure S1A) indicated that the stability of all the MIL-47(V)-X MOFs could be guaranteed to at least 300°C, with little difference between the substituted linkers.[14c] Moreover, the UV/Vis absorption spectra of MIL-47(V)-X MOFs were also recorded and depicted in Figure S1B. The specific peak maxima around ≈350 nm and 400 nm for the MIL-47(V)-NH_2 and MIL-47(V)-OH MOFs are induced by the introduction of the amino and hydroxyl groups on the BDC linker, respectively, in accordance with previous studies.[15] The X-ray photoelectron spectroscopy (XPS) analysis confirmed the presence of elements V, C, and O in all of the MOFs and N, F, and Br in the NH_2-, F-, and Br-substituted MOFs (Figure S1C). Their morphologies were determined by using scanning electron microscopy (SEM) and transmission electron microscopy (TEM). As shown in Figure S2 with different magnifications, the synthesized MOF particles are discrete with different sizes of ≈20–1000 nm.

After successful fabrication of MIL-47(V)-X MOFs, their GPx-mimicking catalytic activities were investigated through monitoring the absorbance change at 340 nm of nicotinamide adenine dinucleotide phosphate (NADPH). In this assay, MIL-47(V)-X catalytically couples the reduction of H_2O_2 to the oxidation of glutathione (GSH) to glutathione disulfide (GSSG). Glutathione reductase (GR) then consumes NADPH to catalyze the reduction of GSSG back to GSH, leading to an observed decrease in the characteristic absorption peak of NADPH (Figure 2B). As shown in Figure 2C and 2D, each of the MIL-47(V)-X MOFs exhibited GPx-mimicking activities, with MIL-47(V)-NH_2, MIL-47(V)-F, and MIL-47(V)-Br having the highest activities among these isostructural MOFs. Of these, MIL-47(V)-NH_2 showed a slightly higher activity than the other two. The superoxide dismutase (SOD)-mimicking and hydroxyl radical scavenging activities of these isostructural MIL-47(V)-X MOFs were also system-
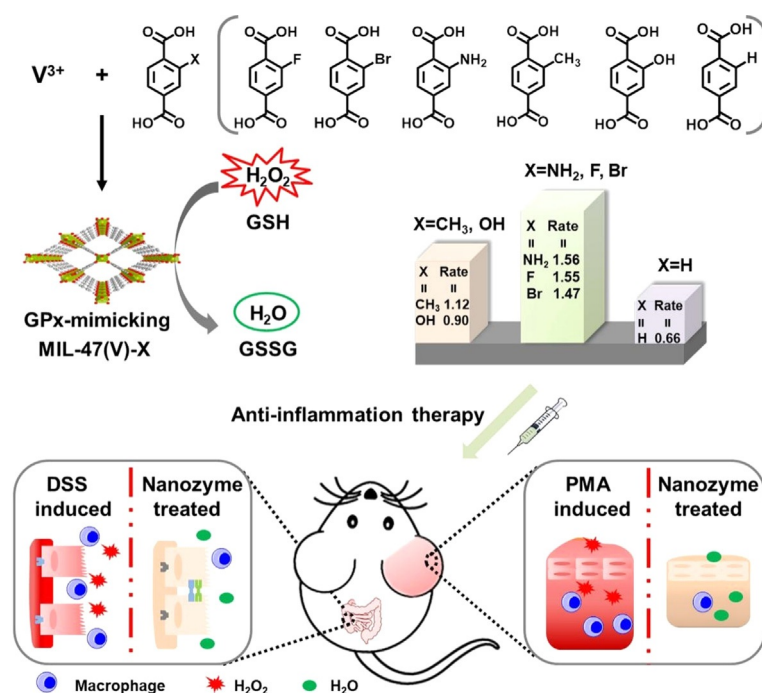

Figure 1. Illustration of the synthesis of rationally designed GPx-mimicking MIL-47(V)-X MOF nanozymes for anti-inflammation therapy. Substituted terephthalate linkers (X = F, Br, NH_2, CH_3, OH, and H) were used to coordinate with vanadium metal ions to form isostructural MIL-47(V)-X MOFs with modulated GPx-mimicking activities. Among them, MIL-47(V)-NH_2 had the highest GPx-mimicking activity and was selected for further investigation in anti-inflammation therapy. Its excellent antioxidation ability can effectively attenuate inflammation in both ear-inflammation and colitis models.
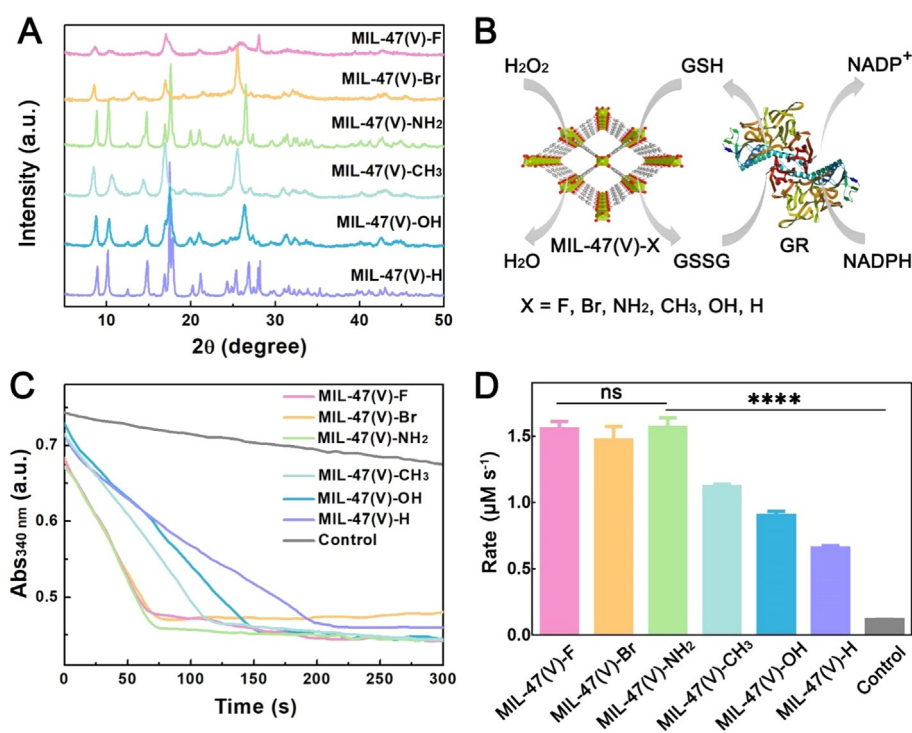
Figure 2. A) PXRD patterns of MIL-47(V)-X MOFs. B) Scheme of reactions catalyzed by GPx-mimicking MIL-47(V)-X MOF nanozymes coupled with glutathione reductase (GR, PDB ID: 3GRS). C) Time evolution of absorbance at 340 nm ($A_{340\,nm}$) for monitoring the GPx-mimicking catalytic activities of MIL-47(V)-X MOFs, under the condition of 50 mM phosphate buffer (pH 7.4) containing 2 mM GSH, 0.4 mM H_2O_2, and 0.4 mM NADPH at room temperature. D) Comparison of GPx-mimicking activities of MIL-47(V)-X MOFs. Control means in the absence of MOF. $X = F$, Br, NH_2, CH_3, OH, and H. MIL-47(V) was written as MIL-47(V)-H for a clear view of the substituent. Data are expressed as mean ± standard error of 3 experiments. **** means $P < 0.0001$ vs. MIL-47(V)-NH_2 MOF, ns means $P > 0.05$ vs. MIL-47(V)-NH_2 MOF.

atically evaluated. Under the same concentration of MIL-47(V)-X MOFs as GPx-mimicking activity test, very low SOD-mimicking activities and negligible hydroxyl radical scavenging activities were observed (Figure S3A and S3B). These results suggest that MIL-47(V)-X MOFs could effectively eliminate H_2O_2 selectively over superoxide or hydroxyl radicals.

To confirm that the GPx-mimicking activity was from the metal nodes of MOFs rather than the substituted ligands, control experiments with only the ligands were performed under the same conditions. As shown in Figure S4, the ligands possess no innate catalytic activity. It is apparent that all the metal nodes in MIL-47(V)-X MOFs rather than the corresponding substituted ligands contributed to the catalytic activities, and large channels present in MIL-47(V) made the metal nodes accessible to the substrates. Thus, the observed catalytic activity difference of MIL-47(V)-X MOFs was inferred to be due to the substitution-induced electronic effect on the metal nodes. XPS analysis in Figure S1D and Table S2 revealed that though the V oxidation state in all MIL-47(V)-X MOFs was V^{III}, the -NH_2, -F, and -Br substitution made the V less oxidized than that in -OH, -CH_3, and -H. According to the previous studies, interaction with H_2O_2 to form the vanadium peroxido intermediate was the first and key step for the catalytic reaction.[7a,9] Thus, compared with

MIL-47(V)-OH, MIL-47(V)-CH_3, and MIL-47(V)-H, the less oxidized V in MIL-47(V)-NH_2, MIL-47(V)-F, and MIL-47(V)-Br is more capable of reacting with H_2O_2, leading to an enhanced catalytic activity. To conclude this part, MIL-47(V)-X MOFs were first reported to behave as GPx-mimicking nanozymes, and high-performance MIL-47(V)-NH_2 was selected for further biological study.

Prior to employing MIL-47(V)-NH_2 in biological experiments, we investigated the effects of substrate and catalyst concentration on the reaction kinetics. As shown in Figure S5, the GPx-mimicking activity increases gradually with increasing concentration of GSH (0–2 mM), H_2O_2 (0–400 μM), and MIL-47(V)-NH_2 (0–80 μg mL^{-1}). The apparent steady-state kinetic parameters (Table S1), the Michaelis constant K_m and the maximal reaction velocity v_{max}, for GSH and H_2O_2 are ≈ 2.85 mM and ≈ 0.0035 mM s^{-1}, ≈ 0.003 mM and ≈ 0.0019 mM s^{-1}, respectively. Based on these results, the 20, 50, and 80 μg mL^{-1} concentrations of MIL-47(V)-NH_2 were selected for further in vitro and in vivo studies.

Before investigating the potential biological applications of the MIL-47(V)-NH_2 MOF nanozyme, its excellent GPx-mimicking activity encouraged us to assess the cytoprotection effect and in vitro ROS scavenging ability (Figure 3A). First, cytotoxicity experiments were performed to assess the biocompatibility of MIL-47(V)-NH_2 MOF nanozyme. As shown in Figure 3B, after 24 h incubation with 0–100 μg mL^{-1} of MIL-47(V)-NH_2 MOF, cell viability was retained at 90%, demonstrating that the MIL-47(V)-NH_2 MOF within 100 μg mL^{-1} exhibited negligible cytotoxicity. Subsequently, the cell protective ability of MIL-47(V)-NH_2 MOF nanozyme against oxidative stress induced by H_2O_2 was studied. As seen in Figure 3C, H_2O_2 treatment caused cell death while MIL-47(V)-NH_2 MOF alleviated the oxidative stress-induced cell death gradually with the increase of MIL-47(V)-NH_2 MOF; 80 μg mL^{-1} of cells had viability nearly equal to the control. The intracellular ROS scavenging ability of MIL-47(V)-NH_2 MOF was monitored with 2′,7′-dichlorofluorescein diacetate (DCFH-DA) as an intracellular ROS fluorescent probe. ROS were generated by lipopolysaccharide (LPS), as indicated by the remarkable fluorescent signal compared to controls (Figure 3D; Figure S6). The fluorescent intensity of DCFH-DA then significantly decreased by 36% with 20 μg mL^{-1} MIL-47(V)-NH_2 MOF treatment. And the more GPx-mimicking MIL-47(V)-NH_2 MOF nanozyme that was added, the
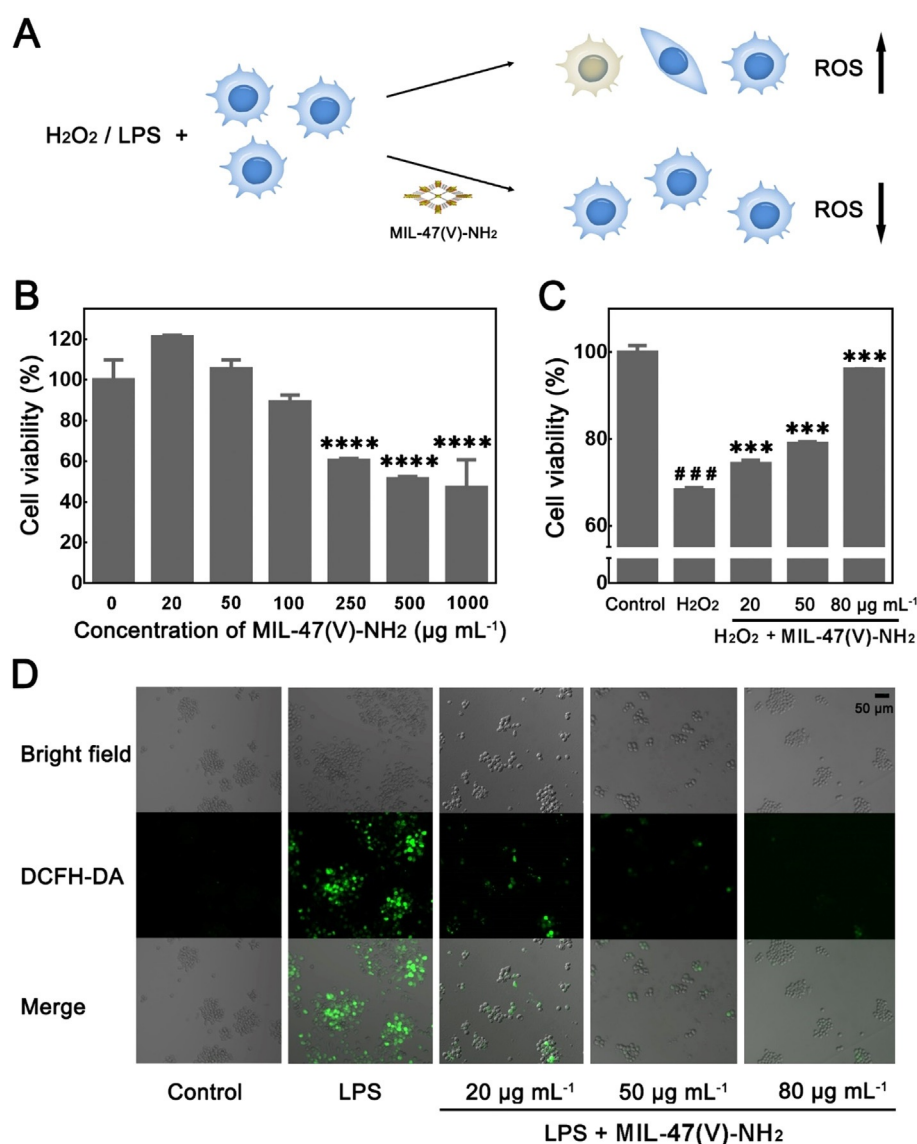
Figure 3. A) Illustration of cytoprotection. B) Cell viability under different concentrations of MIL-47(V)-NH$_2$ MOF. Data are expressed as mean $\pm$ standard error of 3 experiments. **** means $P < 0.0001$ vs. no MIL-47(V)-NH$_2$ MOF-treated group. C) The cytoprotection ability of MIL-47(V)-NH$_2$ MOF. Data are expressed as mean $\pm$ standard error of 3 experiments. ### means $P < 0.001$ vs. control group. *** means $P < 0.001$ vs. H$_2$O$_2$ group. D) Fluorescence microscopy images of cells under different treatments.

as IL-10, IL-4, and Arg-1.[16] The qPCR analysis showed an approximately five hundred times increase of IL-1β mRNA expression (Figure 4A), four hundred times increase of iNOS (Figure 4B), and forty times increase of TNF-α (Figure 4C) when treated with LPS. These elevated markers demonstrated the inflammatory conditions and M1 polarization of macrophages induced by LPS, as previously reported.[17] When subsequently treated with MIL-47(V)-NH$_2$ MOF, mRNA expression levels of pro-inflammatory M1 markers decreased considerably (Figure 4A–C) while expression levels of anti-inflammatory M2 markers (IL-10, IL-4, and Arg-1) were notably enhanced in a dose-dependent manner (Figure 4D–F). Therefore, MIL-47(V)-NH$_2$ MOF was verified to successfully induce the M1 to M2 phenotypic polarization of macrophages and displayed satisfactory in vitro anti-inflammation activity.

Motivated by the above in vitro results, the in vivo anti-inflammation activity of MIL-47(V)-NH$_2$ MOF nanozyme was assessed with a murine ear-inflammation model. First, phorbol 12-myristate 13-acetate (PMA) was applied to the right ear of a mouse to induce ear inflammation (Figure 5A). As shown in Figure S7, the right ear was visibly red and swollen for the pre-treated mouse, indicating that ear inflammation was successfully established. The ear inflammation also led to hyperthermia, as evidenced by $\approx 3\,°C$ increase of right ear temperature in the PMA group as compared to the control group (Figure S8). Varying concentrations of MIL-47(V)-NH$_2$ MOF were then subcutaneously injected in the inflamed ear for treatment. The in vivo ROS scavenging activity of MIL-47(V)-NH$_2$ MOF nanozyme are shown in Figure 5B and Figure S9, based on the fluorescence intensity of the ROS probe DCFH-DA. The reduction in DCFH-DA fluorescence was observed to be dose-dependent and the corresponding ear tissue sections stained with hematoxylin and eosin (H&E) also demonstrated a dose-dependent antioxidation effect of MIL-47(V)-NH$_2$ MOF with the inflammatory response effectively alleviated at the highest dose (Figure 5C). The relieved inflammation made the right ear temperature decrease by $\approx 2\,°C$ as well (Figure S8). When comparing with the

more the fluorescence intensity of DCFH-DA decreased. Together, these results show MIL-47(V)-NH$_2$ MOF to not only possess good biocompatibility, but also to be an effective ROS scavenger that protects cells from oxidative damage.

We also evaluated the effect of MIL-47(V)-NH$_2$ MOF on the polarization of macrophages from the M1 to M2 phenotype. Macrophages play a prominent part in innate immunity as the first line of the host immune system. Macrophages typically exist in a dormant state, M0, and switch to the activated M1 state, releasing inflammatory factors such as IL-1β, iNOS, and TNF-α, when facing bacterial infection or other stimulations. Macrophages can also adopt the activated M2 phenotype to promote tissue repair and wound healing by releasing anti-inflammatory cytokines such
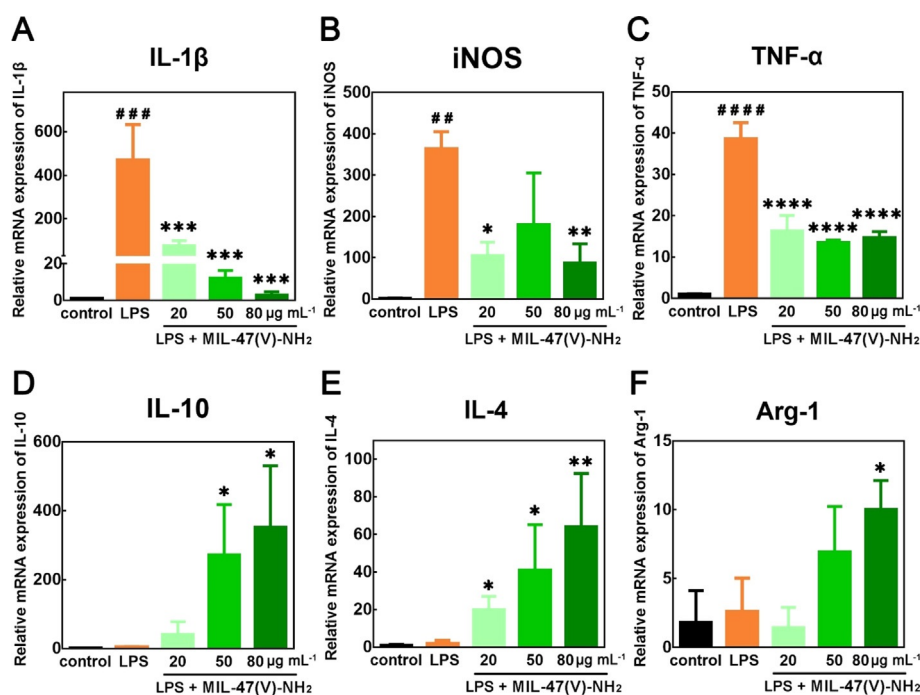
Figure 4. mRNA expression levels of M1 and M2 markers in the LPS-induced macrophages receiving different concentrations of MIL-47(V)-NH$_2$ nanozyme. A) IL-1β, B) iNOS, C) TNF-α, D) IL-10, E) IL-4, and F) Arg-1 levels under different treatments. Data are expressed as mean ± standard error of 3 experiments. #### means $P < 0.0001$ vs. control group. ### means $P < 0.001$ vs. control group. ## means $P < 0.01$ vs. control group. **** means $P < 0.0001$ vs. LPS group. *** means $P < 0.001$ vs. LPS group. ** means $P < 0.01$ vs. LPS group. * means $P < 0.05$ vs. LPS group.
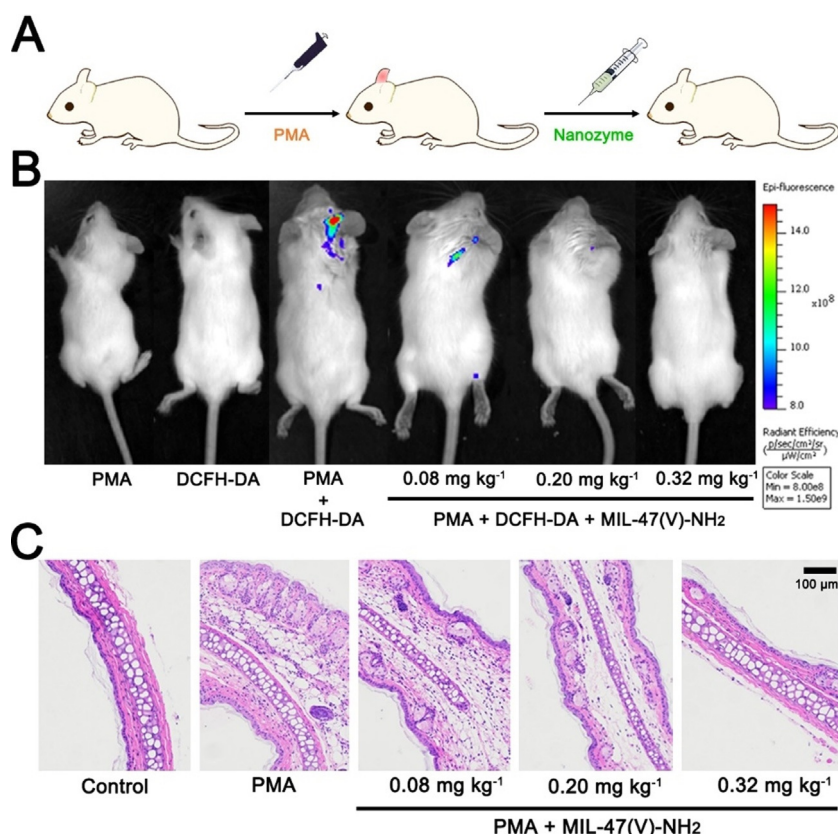

Figure 5. A) Illustration of an ear-inflammation model. B) In vivo fluorescence imaging of mice with PMA-induced ear inflammation after different treatments. C) H&E-stained images of ear tissue after different treatments.

MIL-47(V)-H MOF nanozyme (Figures S9 and S10), the MIL-47-(V)-NH$_2$ MOF with a better GPx-mimicking activity exhibited greater anti-inflammation capability, especially at low dosage. These results suggested that the rationally designed MIL-47(V)-NH$_2$ MOF nanozyme had elevated ROS scavenging capacity and enhanced the in vivo anti-inflammation efficacy. Moreover, a commercial anti-inflammation drug dexamethasone (Dex) was applied in the ear-inflammation model as well. Both the reduced (around −98 %) in vivo DCFH-DA fluorescence intensity and the corresponding ear tissue section stained with H&E indicated that the therapeutic efficacy of Dex was comparable to that of MIL-47(V)-NH$_2$ under the same dosage (Figure S11). After the treatment, no obvious histological changes or inflammatory damage of major organs including liver, spleen, and kidney of the mice were observed (Figure S12), indicating good in vivo biocompatibility of our MOF nanozymes. Together, these results reveal that GPx-mimicking MIL-47(V)-NH$_2$ MOF nanozyme possesses excellent in vivo anti-inflammatory activity and effectively protects against oxidative stress damage.

To further evaluate the in vivo anti-inflammation effect of MIL-47(V)-NH$_2$ beyond treatment of superficially inflamed ears, we also established an acute dextran sulfate sodium (DSS)-induced colitis model, as a typical refractory chronic inflammatory bowel disease associated with overproduced ROS.[18] As shown in Figure 6A, DSS was administered by feeding over six days, followed by intraperitoneal administration of MIL-47(V)-NH$_2$ MOF nanozyme once per day for three consecutive days. Subsequently, the colon was collected to evaluate the therapeutic efficacy on the tenth day. The body weight of each mouse was recorded daily during this process with the body weights of all DSS-induced groups decreasing, indicating the successful establishment of a colitis model, as shown in Figure 6B. Upon treatment with MIL-47(V)-NH$_2$ nanozyme, the body weights of the mice gradually recovered, suggesting that the anti-inflammatory effect of MIL-47(V)-NH$_2$ extends to colitis
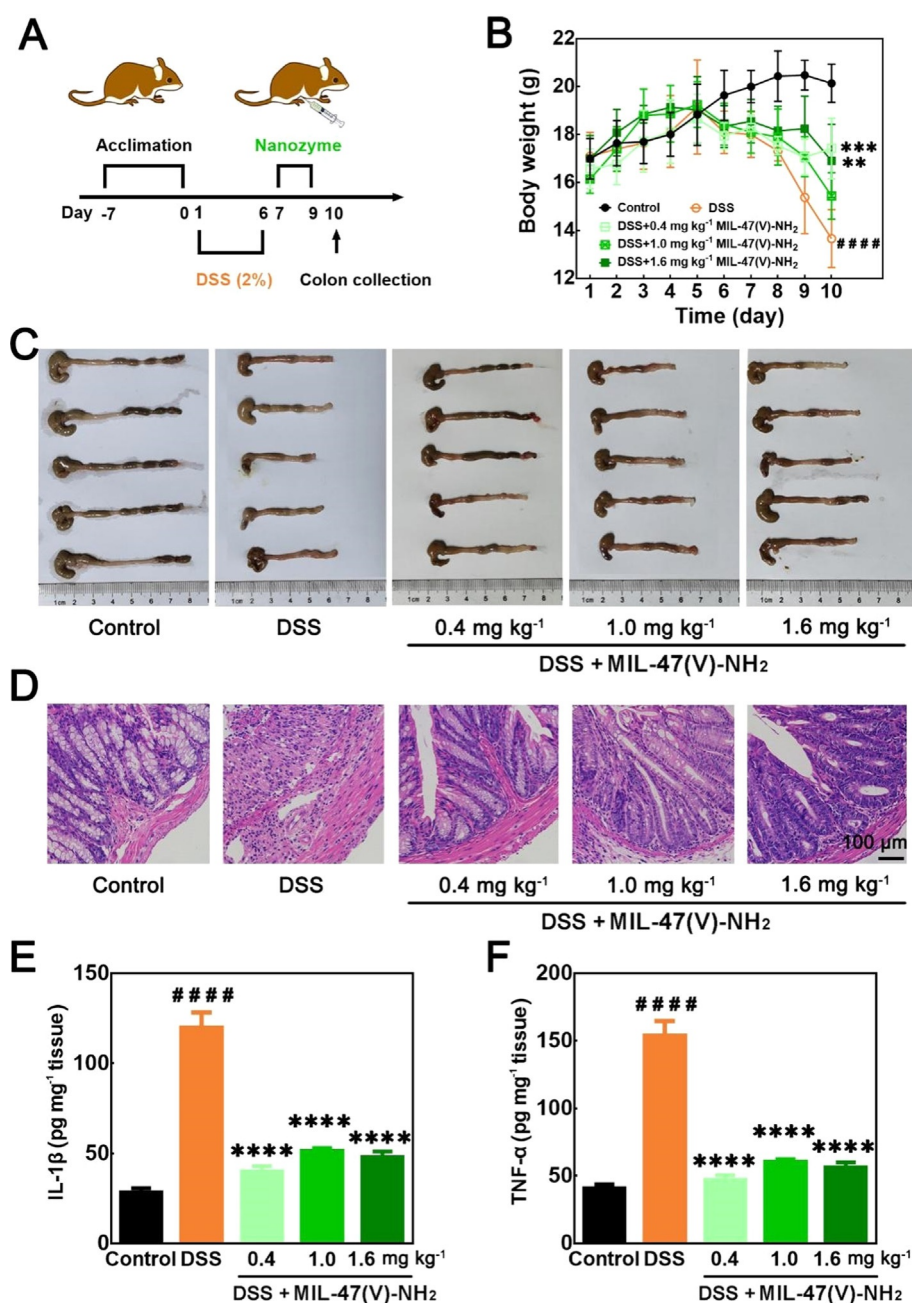
Figure 6. A) Illustration of the establishment and treatment procedure of the colitis model. B) Daily body weight recorded under different treatments. C) Images of the colons taken on day 10. D) H&E-stained images of colons under different treatments. E) IL-1β and F) TNF-α levels in colon homogenates under different treatments. Data are expressed as mean ± standard error of 5 experiments. #### means $P < 0.0001$ vs. control group. ** means $P < 0.01$ vs. DSS group. *** means $P < 0.001$ vs. DSS group. **** means $P < 0.0001$ vs. DSS group.

consistent with the phenomena of the in vitro study (Figure 4). These results strongly suggest that the MIL-47(V)-NH_2 nanozyme significantly down-regulated the levels of inflammatory cytokines IL-1β and TNF-α, and thus effectively mitigated colonic inflammation.

Similar to the findings in the ear-inflammation model, the MIL-47(V)-NH_2 MOF demonstrated greater anti-inflammatory activity than the less active MIL-47(V)-H nanozyme (Figures S13 and S14). Notably, for the MIL-47(V)-NH_2 nanozyme, the therapeutic efficacy under three different concentrations was similar, suggesting that the treatment of MIL-47(V)-NH_2 at 0.4 mg kg^{-1} was effective enough for therapy. For the less active MIL-47(V)-H nanozyme, a positive correlation between the therapeutic efficacy and the treated concentrations was revealed, and only at the highest dose of 1.6 mg kg^{-1} was the therapeutic efficacy comparable to that of MIL-47(V)-NH_2 nanozyme. The above results not only verified that a high performance GPx-mimicking nanozyme alone could be applied in anti-inflammation therapy, but also advanced nanozyme-based therapy studies, where the structure–activity regulation of the nanozyme could be explored to guide in vivo therapy. Moreover, a clinical small-molecule drug 5-aminosalicylic acid (5-ASA) was applied in our model. The slight down-regulated levels (around −20%) of inflammatory cytokines (Figure S13C and S13D) and corresponding colon tissue section stained with H&E (Figure S14) indicated that the therapeutic efficacy of 5-ASA was weaker than that of both MIL-47(V)-NH_2 and MIL-47-(V)-H nanozymes under the same dosage of 1.0 mg kg^{-1}. No distin-

treatment. Colon length (Figure 6C; Figure S13) and corresponding colon sections stained with H&E (Figure 6D) also suggested that the inflammatory response was effectively alleviated after the administration of MIL-47(V)-NH_2 nanozyme, as compared with the shortened colon length and inflamed colon tissue in the DSS group. Further, the significant down-regulated levels (around −60%) of inflammatory cytokines IL-1β (Figure 6E) and TNF-α (Figure 6F) in MIL-47(V)-NH_2 nanozyme treated group were observed, which were just a little higher than the control group,

guishable tissue damage or inflammatory lesions of other organs, including heart, lung, liver, spleen, and kidney in mice were observed in either nanozyme therapy (Figure S15), further supporting the good in vivo biocompatibility of our MOFs. Therefore, these results demonstrate that the high-performance MIL-47(V)-NH_2 nanozyme could relieve inflammatory bowel disease, indicating a promising potential of MIL-47(V)-NH_2 as an efficient nanomedicine for anti-inflammation therapy.

1232   www.angewandte.org

© 2020 Wiley-VCH GmbH

Angew. Chem. Int. Ed. 2021, 60, 1227–1234

Conclusion

In summary, we have successfully synthesized MOF nanozymes with GPx-mimicking activities, which to our knowledge is the first report of GPx-mimicking MOF nanozymes. Even though both nanozymes and biomimetic MOFs have been widely studied for more than 20 years, few studies have reported GPx-mimicking nanozymes, especially GPx-mimicking MOF nanozymes. By using vanadium metal nodes and (substituted) terephthalate linkers, MIL-47(V)-X (X = F, Br, NH_2, CH_3, OH, and H) MOFs were successfully fabricated with rationally regulated GPx-mimicking activities. With the best performing example, we demonstrated the use of MIL-47(V)-NH_2 as a ROS scavenger in vitro, which protected cells from oxidative damage. This result was extended to in vivo anti-inflammation, demonstrating a broad-spectrum anti-inflammatory effect toward both ear-inflammation and colitis. Moreover, the therapeutic efficacy of the highly active MIL-47(V)-NH_2 was superior to that of the less active MIL-47(V)-H. These results not only verify that a GPx-mimicking nanozyme alone can be applied in anti-inflammation therapy, but also demonstrate that traditional concepts of structure–activity relationships can be applied in the design of nanozyme-based therapies. Thus, the study of GPx-mimicking MOF nanozymes has the potential to greatly expand the range of biomimetic MOFs, allowing this class of antioxidant nanozymes to enrich the current nanozyme research.

Acknowledgements

Conflict of interest

The authors declare no conflict of interest.

Keywords: activity modulation · anti-inflammation therapy · glutathione peroxidase mimics · ligand engineering strategies · metal–organic frameworks

[1] C. C. Winterbourn, *Nat. Chem. Biol.* **2008**, *4*, 278–286.
[2] G. P. Bienert, A. L. B. Møller, K. A. Kristiansen, A. Schulz, I. M. Møller, J. K. Schjoerring, T. P. Jahn, *J. Biol. Chem.* **2007**, *282*, 1183–1192.
[3] E. Lubos, J. Loscalzo, D. E. Handy, *Antioxid. Redox Signaling* **2011**, *15*, 1957–1997.
[4] a) X. Huang, X. Liu, Q. Luo, J. Liu, J. Shen, *Chem. Soc. Rev.* **2011**, *40*, 1171–1184; b) K. P. Bhabak, G. Mugesh, *Acc. Chem. Res.* **2010**, *43*, 1408–1419; c) H. Xu, W. Cao, X. Zhang, *Acc. Chem. Res.* **2013**, *46*, 1647–1658.
[5] a) L. Z. Gao, J. Zhuang, L. Nie, J. B. Zhang, Y. Zhang, N. Gu, T. H. Wang, J. Feng, D. L. Yang, S. Perrett, X. Y. Yan, *Nat. Nanotechnol.* **2007**, *2*, 577–583; b) H. Wei, E. K. Wang, *Chem. Soc. Rev.* **2013**, *42*, 6060–6093; c) J. Wu, X. Wang, Q. Wang, Z. Lou, S. Li, Y. Zhu, L. Qin, H. Wei, *Chem. Soc. Rev.* **2019**, *48*, 1004–1076.
[6] a) F. Natalio, R. André, A. F. Hartog, B. Stoll, K. P. Jochum, R. Wever, W. Tremel, *Nat. Nanotechnol.* **2012**, *7*, 530–535; b) G. Y. Tonga, Y. Jeong, B. Duncan, T. Mizuhara, R. Mout, R. Das, S. T. Kim, Y.-C. Yeh, B. Yan, S. Hou, V. M. Rotello, *Nat. Chem.* **2015**, *7*, 597–603; c) W. Zhang, S. Hu, J.-J. Yin, W. He, W. Lu, M. Ma, N. Gu, Y. Zhang, *J. Am. Chem. Soc.* **2016**, *138*, 5860–5865; d) Z. Zhang, X. Zhang, B. Liu, J. Liu, *J. Am. Chem. Soc.* **2017**, *139*, 5412–5419; e) M. Soh, D.-W. Kang, H.-G. Jeong, D. Kim, D. Y. Kim, W. Yang, C. Song, S. Baik, I.-Y. Choi, S.-K. Ki, H. J. Kwon, T. Kim, C. K. Kim, S.-H. Lee, T. Hyeon, *Angew. Chem. Int. Ed.* **2017**, *56*, 11399–11403; *Angew. Chem.* **2017**, *129*, 11557–11561; f) M. S. Kim, S. Cho, S. H. Joo, J. Lee, S. K. Kwak, M. I. Kim, J. Lee, *ACS Nano* **2019**, *13*, 4312–4321; g) L. Huang, J. Chen, L. Gan, J. Wang, S. Dong, *Sci. Adv.* **2019**, *5*, eaav5490; h) C. N. Loynachan, A. P. Soleimany, J. S. Dudani, Y. Lin, A. Najer, A. Bekdemir, Q. Chen, S. N. Bhatia, M. M. Stevens, *Nat. Nanotechnol.* **2019**, *14*, 883–890.
[7] a) S. Ghosh, P. Roy, N. Karmodak, E. D. Jemmis, G. Mugesh, *Angew. Chem. Int. Ed.* **2018**, *57*, 4510–4515; *Angew. Chem.* **2018**, *130*, 4600–4605; b) N. Singh, M. A. Savanur, S. Srivastava, P. D'Silva, G. Mugesh, *Angew. Chem. Int. Ed.* **2017**, *56*, 14267–14271; *Angew. Chem.* **2017**, *129*, 14455–14459; c) Y. Y. Huang, C. Q. Liu, F. Pu, Z. Liu, J. S. Ren, X. G. Qu, *Chem. Commun.* **2017**, *53*, 3082–3085.
[8] a) Y. Huang, Z. Liu, C. Liu, Y. Zhang, J. Ren, X. Qu, *Chem. Eur. J.* **2018**, *24*, 10224–10230; b) Y. Y. Huang, Z. Liu, C. Q. Liu, E. G. Ju, Y. Zhang, J. S. Ren, X. G. Qu, *Angew. Chem. Int. Ed.* **2016**, *55*, 6646–6650; *Angew. Chem.* **2016**, *128*, 6758–6762; c) T. Liu, B. Xiao, F. Xiang, J. Tan, Z. Chen, X. Zhang, C. Wu, Z. Mao, G. Luo, X. Chen, J. Deng, *Nat. Commun.* **2020**, *11*, 2788.
[9] A. A. Vernekar, D. Sinha, S. Srivastava, P. U. Paramasivam, P. D'Silva, G. Mugesh, *Nat. Commun.* **2014**, *5*, 5301.
[10] a) H. Deng, C. J. Doonan, H. Furukawa, R. B. Ferreira, J. Towne, C. B. Knobler, B. Wang, O. M. Yaghi, *Science* **2010**, *327*, 846–850; b) M. Zhao, K. Yuan, Y. Wang, G. Li, J. Guo, L. Gu, W. Hu, H. Zhao, Z. Tang, *Nature* **2016**, *539*, 76–80; c) S. Kitagawa, *Acc. Chem. Res.* **2017**, *50*, 514–516; d) L. He, G. Huang, H. Liu, C. Sang, X. Liu, T. Chen, *Sci. Adv.* **2020**, *6*, eaay9751; e) T. M. Rayder, E. H. Adillon, J. A. Byers, C.-K. Tsung, *Chem* **2020**, *6*, 1742–1754.
[11] a) K. Chen, C.-D. Wu, *Coord. Chem. Rev.* **2019**, *378*, 445–465; b) I. Nath, J. Chakraborty, F. Verpoort, *Chem. Soc. Rev.* **2016**, *45*, 4127–4170; c) M. Zhang, Z.-Y. Gu, M. Bosch, Z. Perry, H.-C. Zhou, *Coord. Chem. Rev.* **2015**, *293–294*, 327–356.
[12] P. Van Der Voort, K. Leus, Y.-Y. Liu, M. Vandichel, V. Van Speybroeck, M. Waroquier, S. Biswas, *New J. Chem.* **2014**, *38*, 1853–1867.
[13] a) A. Centrone, T. Harada, S. Speakman, T. A. Hatton, *Small* **2010**, *6*, 1598–1602; b) M. Vandichel, S. Biswas, K. Leus, J. Paier, J. Sauer, T. Verstraelen, P. Van Der Voort, M. Waroquier, V. Van Speybroeck, *ChemPlusChem* **2014**, *79*, 1183–1197.
[14] a) K. Barthelet, J. Marrot, D. Riou, G. Férey, *Angew. Chem. Int. Ed.* **2002**, *41*, 281–284; *Angew. Chem.* **2002**, *114*, 291–294; b) K. Leus, S. Couck, M. Vandichel, G. Vanhaelewyn, Y.-Y. Liu, G. B. Marin, I. V. Driessche, D. Depla, M. Waroquier, V. V. Speybroeck, J. F. M. Denayer, P. Van Der Voort, *Phys. Chem. Chem. Phys.* **2012**, *14*, 15562–15570; c) S. Biswas, D. E. P. Vanpoucke,

T. Verstraelen, M. Vandichel, S. Couck, K. Leus, Y.-Y. Liu, M. Waroquier, V. Van Speybroeck, J. F. M. Denayer, P. Van Der Voort, *J. Phys. Chem. C* **2013**, *117*, 22784–22796.

[15] Y. Fu, D. Sun, Y. Chen, R. Huang, Z. Ding, X. Fu, Z. Li, *Angew. Chem. Int. Ed.* **2012**, *51*, 3364–3367; *Angew. Chem.* **2012**, *124*, 3420–3423.

[16] a) D. Zhou, C. Huang, Z. Lin, S. Zhan, L. Kong, C. Fang, J. Li, *Cell. Signalling* **2014**, *26*, 192–197; b) S. Gordon, F. O. Martinez, *Immunity* **2010**, *32*, 593–604.

[17] M. Schieber, N. S. Chandel, *Curr. Biol.* **2014**, *24*, R453–R462.

[18] J. M. Knipe, L. E. Strong, N. A. Peppas, *Biomacromolecules* **2016**, *17*, 788–797.